Winter Equatorial Warming in Martian Upper Atmosphere from MAVEN Densities

Jiandong Liu[1,2,3],Yawen Li[1], Peng Han[1], Ehouran Millour[4], Haibing Ruan[1], Shuanggen Jin[1,2*]

[1]School of Remote Sensing and Geomatics Engineering, Nanjing University of Information Science and Technology, Nanjing 210044, China

[2]Key Laboratory of Planetary Science, Shanghai Astronomical Observatory, Chinese Academy of Sciences,Shanghai 200030, China

[3]University of Chinese Academy of Sciences, Beijing 100049, China

[4]Laboratoire de Météorologie Dynamique, IPSL Université Pierre et Marie Curie,Paris 75005, France

Key Points:

- A new phenomenon of higher density distribution in Mars equatorial region is reported.
- The feature appears in both mass density and five major species abundances during day and night.
- The longitudinal structure of the equatorial warming region is orographic-related.

Corresponding author: Shuanggen Jin, sgjin@shao.ac.cn;sgjin@nuist.edu.cn

Abstract

Martian upper atmosphere warming reflects the energy-materials interactions from the lower atmosphere layers. In this paper, we show a new phenomenon that enhances Mars upper atmosphere density in the equatorial region during the winter periods. First, both accelerometer-derived density and NGIMS-measured species from MAVEN show that the winter equatorial region has a secondary warming peak compared with that of the high-latitude polar warming area. Second, the major neutrals (CO2, Ar, CO, N2, and O) indicate that the phenomenon extends at least up to 240 km during both day and night sides. Furthermore, the topographic-related longitudinal structure emerged in the equatorial sector indicates that the variations are more dynamical than we expected. The warming found in this study suggest to be dust-related and influenced by the evolution of the seasonal solar insolation. Both local factors, upward small-scale gravity waves and CO2 IR-thermal effect transfer, may play key roles in shaping the warming structure.

Plain Language Summary

The term 'warming' in Mars upper-layer (altitude $>$ 100 km) represents abnormal higher density distribution in a specific region. This paper reports a 'warming' region that locates at Martian north hemisphere winter equatorial zone (30° S$<$latitude $<$ 30°N) using MAVEN densities (MGS,ODY and MRO accelerometer-derived densities are also used for altitude between 100 to 150 km). Generally, the winter equatorial zone was predicted extremely cold by models because the cooling effects triggered by the expanding of background CO2 abundances due to the winter dust storms. We found that the equatorial warming, together with polar warming, can be observed in mass density and volatiles abundances. Additionally, the variation of the warming in the longitude direction is correlated with the Martian unique topography at an altitude of at least 170 km, which is a uncommon phenomenon (the effect was thought only can be observed within altitude 50 km). We suggested the overall warming structure described in this paper is a kind of global atmospheric circulation pattern during Mars winter. The latitudinal variation inside the warming structure could be major triggered by the small-scale gravity waves and modulated by the cooling effects generated by the background CO2 enhancement during the winter dust expansion.

1 Introduction

In the past two decades, the aspect of complex variations of Mars upper atmosphere has been recognized by accelerometer(ACC)-derived (e.g., Withers, 2006; Tolson et al., 2008; R. W. Zurek et al., 2015, and others) and Neutral Gas and Ion Mass Spectrometer (NGIMS)-measured density (e.g., Mahaffy et al., 2015; S. W. Bougher et al., 2017) from several orbiters. One of the most interesting phenomenon captured by these densities is that the thermosphere has strong responses to the lower atmospheric activities such as surface dust storms especially during the dust seasons (Ls 135°-360°) (e.g., Keating et al., 1998), triggering enhancement of density in thermosphere(Jain et al., 2020) and accelerating the escape of the upper volatiles (Fang et al., 2020). Therefore, the understanding of abnormal density distribution in a specific area of the upper layers could benefit the understanding of the mechanisms of energy transportation and atmospheric circulation from the lower layers to the magnetosphere-ionosphere-thermosphere system.

The recent Mars Atmospheric and Volatile EvolutioN (MAVEN) orbiter has made comprehensive observations of the upper layers (Jakosky, Lin, et al., 2015), which gives deep insight into the functions of the complex variations. The impacts (e.g., dust storms, dynamical processes, gravity waves, etc.) from lower layers (e.g., S. England et al., 2017; Benna et al., 2019; Jain et al., 2020), the driving forces from the Solar irradiations/winds (e.g., Jakosky, Grebowsky, et al., 2015), and the corresponding coupling in this region (e.g., Fang et al., 2020) triggered complex density distribution, in which the autumn-winter (all seasons mentioned by this paper refers to the Martian north hemisphere) 'Polar Warming' was detected by these observations (J. Liu et al., 2019; Felici et al., 2020). The term 'warming', which is always due to thermal energy releasing by dynamical or thermal processes, represents higher density distribution in some particularly localities (Figure 1). By its meaning, the Mars 'Polar Warming' corresponds to higher densities distribution locate in the Martian high-latitude polar region (Figure 1). As well as, the term 'Winter Equatorial Warming' (WEW) substitutes for the higher density distribution around the Mars equatorial sector (30°S to 30°N for this paper) during Mars winter.

The thermospheric 'Polar Warming' was first noticed by Keating et al. (2003) using Mars Global Surveyor (MGS) and Mars Odyssey (ODY) accelerometer-derived density. Afterwards, both observational and theoretic studies shown that the warming could be triggered by several factors in terms of dust impacts(e.g., S. Bougher et al., 2006; Fe-

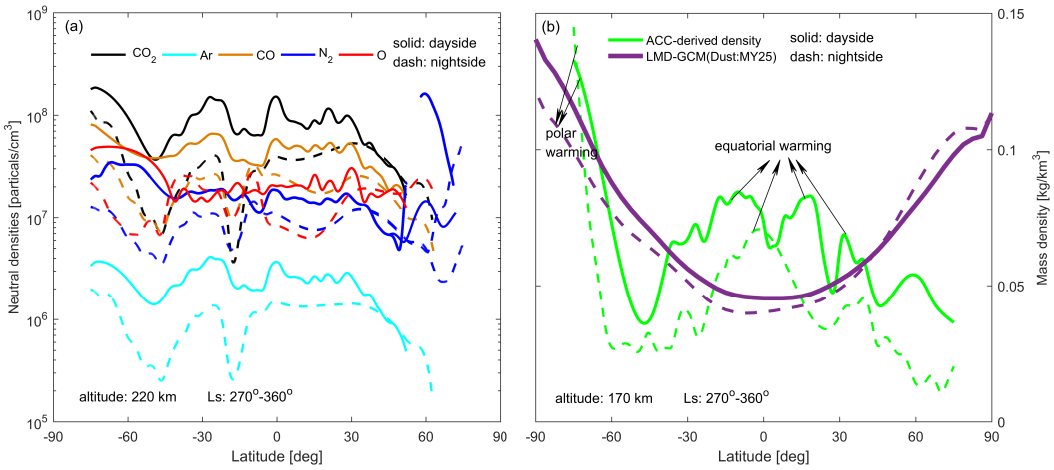

Figure 1. Winter latitudinal structure from MAVEN densities and the LMD-MGCM simulation. (a) average NGIMS neutral densities [CO2,Ar,CO,N2,and O] at altitude of 220 km during Ls 270°-360° (MY32 to MY34). South polar warming is detected in all the five neutrals during both dayside (6 h < LST<18 h, solid lines) and nightside (0 h<LST< 6 h or 18 h<LST< 24 h,dash lines). Winter equatorial warming (30°S<latitude<30°N) exists in all neutrals. An extremely hot north polar region is captured by N2 (blue). (b) the corresponding latitudinal average of ACC-derived density (green) at altitude 170 km and the LMD-MGCM predictions (purple). The polar warming has been addressed by many other orbiters' ACC-derived densities/temperatures (S. Bougher et al., 2006; Forbes & Zhang, 2018). As well as, the deep trough lies in 40°S-60°S or 40°N-70°N is cooled by CO2 radiative transfer in 15 μm frequency band (Medvedev et al., 2015).

lici et al., 2020), seasonal solar irradiation(e.g., Keating et al., 2003; S. Bougher et al., 2006, and others), Internal Atmospheric Gravity Waves(IAGWs) (Medvedev et al., 2015, 2016), trans-hemisphere atmospheric circulations (S. Bougher et al., 2006), and corresponding coupling processes (Medvedev & Yiğit, 2012).

The WEW was neglected due to lack of winter density observations: the ACC-derived densities covered a limited Solar Longitude (Ls) and inadequate global coverage before the MAVEN measurements (both ACC and NGIMS densities) was made. Consequently, the warming described by former researches was isolated profiles, in which the polar warming was highlighted out distinctly yet the 'Winter Equatorial Warming' (WEW) was neglected even though the feature of the phenomenon has been captured by these densities (Figure 1b). Furthermore, the General Circulation Model (MGCM) simulations to interpret the mechanism that drive the 'Polar Warming' always predicted a cold if not extreme cold winter equatorial region (Medvedev & Yiğit, 2012), which is conflicted with the observations as shown in Figure 1b.

In this paper, equatorial warming in Mars winter is reported by ACC and NGIMS densities. The density coverage and the seasonal evolution of Mars upper atmosphere are explained in Section 2. In Section 3, the WEW is illustrated by both ACC-derived densities and abundances of five major upper volatiles (CO2,Ar,CO,N2,and O) sampled by NGIMS. Additionally, the winter longitudinal structure is also illustrated. Both seasonal and local drivers of the WEW are discussed in Section 4. The summary is given in Section 5.

2 Data and Theory

2.1 Densities coverages

We use accelerometer-derived density and Neutral Gas and Ion Mass Spectrometer (NGIMS) measured major species abundances in terms of CO2,Ar,CO,N2 and O from MAVEN spacecraft. Mass densities from Mars Global Surveyor (MGS), Mars Reconnaissance Orbiter (MRO), and Mars Odyssey (ODY) were also used at altitude between 120 and 150 km to valid the WEW features. The data are released by the National Aeronautics and Space Administration Planetary Data System (NASA-PDS) system which is available at: `https://pds-atmospheres.nmsu.edu/data_and_services/atmospheres_data/MARS/mars_orbiter.html`.

The densities covered three Mars Years (MY), i.e., MY32 (Ls: 270°−360°), MY33 (Ls: 0° − 360°), and MY34 (Ls: 0° − 360°). The corresponding dust storm activities strength can be seen in Montabone et al. (2015, 2020) and following section 3.1 and 3.2. The accuracy and the spatial-temporal coverage of the data are described by J. Liu et al. (2019) and Li et al. (2020). The simulations to compare with the observations and density processing are made by Mars General Circulation Model and Mars Climate Database respectively developed in Laboratoire de Météorologie Dynamique (LMD-MGCM/LMD-MCD).

2.2 Global and local drivers for the upper layers

Mars upper atmospheric system is forced by both external inputs that eventually owing to solar irradiation/wind (Jakosky, Grebowsky, et al., 2015) and internal factors such as the surface dust storms (e.g., Fang et al., 2020; Felici et al., 2020, and others) and the Internal Atmospheric Gravity Waves (IAGWs) (Medvedev et al., 2015; S. England et al., 2017; J. Liu et al., 2019) , which is the two major contributors during the seasonal evolution. The seasonal response of the atmospheric density to the contributors is as follows (R. Zurek et al., 2017; J. Liu et al., 2019):

$$\ln \rho = \alpha_0 + \frac{\alpha_1 cosSZA + \alpha_2}{r_{sm}^2} + \alpha_3 Dust_{IR-CDOD} \tag{1}$$

Where $Dust_{IR-CDOD}$, Infra-Red Column Dust Optical Depth (IR-CDOD) index for dust storms (Montabone et al., 2015, 2020), is a wide-used index to evaluate the strength of the dust storms. r_{sm} is the Sun-Mars distance. Wherein α_0 to α_3 are constants. The solar flux of the zenith component could cause density responses that is directly ratio to $\alpha_1 cosSZA + \alpha_2$. SZA, Solar Zenith Angle. The planetary decay of the solar intensity could couple with the local effect, in which the atmospheric density would vary as $exp[\alpha_0 + (\alpha_1 cosSZA + \alpha_2)/r_{sm}^2]$ that has been confirmed by MGS and MAVEN ACC-derived densities (R. Zurek et al., 2017; J. Liu et al., 2019). exp is an exponential function.

In addition to large-scale seasonal divers mentioned above, small-scale local variables can also influence the global density variations. First of all, gravity waves are significant contributors that can influence the Martian thermosphere-exosphere by transfer energy and momentum from lower layers (Yiğit et al., 2015; S. W. Bougher et al., 2017). Internal Atmospheric Gravity Waves (IAGWs) have been detected by MAVEN ACC-derived and NGIMS-measured densities at altitude of 100-220 km (Yiğit et al., 2015; S. Eng-

land et al., 2017; J. Liu et al., 2019), in which the waves are always coupled with the dust storms during the dust seasons (J. Liu et al., 2019; Elrod et al., 2020). Small-scale upward IAGWs has been validated as the major driver for the warming (such as polar warming) of the upper atmosphere by MGCM simulations (Medvedev & Yiğit, 2012) and MAVEN observations (Medvedev et al., 2016). Secondly, the thermal effect of IR transfer by CO2 monoculars can cool down the atmosphere distinctly (Medvedev et al., 2016). This is also illustrated in Figure 1 (the deep gill around 60°S). Additionally, along-tracks winds derived from MAVEN shows that the IAGWs generated by Mars topography could extend to thermosphere directly (Benna et al., 2019), which indicates the upper layers have more intensive responses to the surface processes than we expected.

3 Winter Equatorial Warming

3.1 Overall picture from ACC densities

Several important global features can be seen from the seasonal average of ACC-derived density (Figure 2). The spring and summer ('clear sky' seasons) hemispheric density distribution was thought mainly modulated by the solar term and the topographic effects (Forbes et al., 2002; Forbes & Zhang, 2018, and the series works). Specifically, a warming north spring hemisphere appeared and a wave-3 longitudinal pattern shown up there (G. Liu et al., 2017, and others), which is thought to be a modulation of diurnal solar tide into the Mars typical wave-2 topography. The global assignment of the summer has five levels that are: a relative cooler south polar, a warmest south mid-latitude region, a second-warmest 30°S to equator area, a coolest north low-latitude sector that extends to 45°, and a warm north mid to high-latitude zone. The wave pattern is wave-3 (G. Liu et al., 2017; Terada et al., 2017). All spring and summer features can be owing to the solar term forcing (R. Zurek et al., 2017), trans-hemisphere circulation (S. Bougher et al., 2006), and corresponding topographic modulation (Terada et al., 2017).

The autumn seasons have typical features in latitudinal variations. The autumn density approximates to be symmetric with the hemisphere: An extreme cold region (40°S-40°N) around the equator, where the autumn dust main peaks takes place (Figure 2, IR-CDOD). The structure can be explained as follows: The atmospheric inflation would cause the main species CO2 to expand from lower layers to the upper atmosphere, which could cool down (CO2 IR-thermal effect transfer) the upper layers in the equatorial region. This

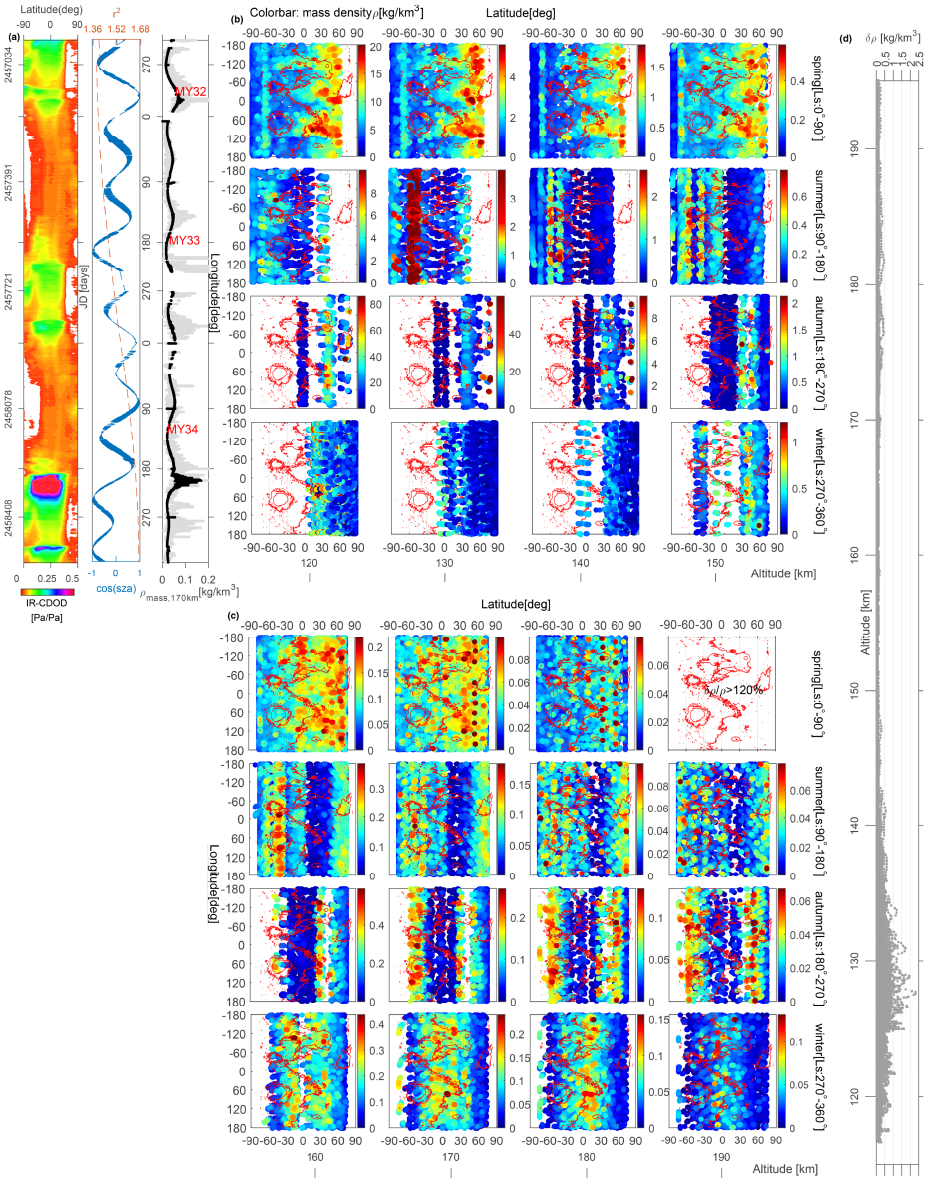

Figure 2. Global view of WEM from ACC-derived density. (a) Seasonal density (ρ_{170km}, gray point) variation forced by solar term with planetary propagation effect ($r^2, cosSZA$) and surface dust storms (IR-CDOD)(Mahaffy et al., 2015). The seasonal evolution (MY32 to MY34) is fit by equation (1)(black line). (b) seasonal global density variation from 120 to 150 km and (c) 160 to 190 km. For the winter season, a distinct south high-latitude warming (170-180 km) and a higher equatorial (30°S to 30°N) density (120-190 km) is captured at both dayside and nightdside. A extremely winter warming in north polar region is also found by MGS,ODY observations at altitude of 120 to 140 km (without colorbar) but is excluded for simplicity. The spring/summer wave-3 longitudinal structure are tidal waves generated by modulation of Mars topography and solar illuminating (e.g, S. L. England et al., 2019; Thaller et al., 2020). (d) $\delta\rho$ is the derived error. The ratio $\delta\rho/\rho$ surpass 100% at altitude of above 180 km during spring and summer seasons, consequently, some of the features are corrupted by the errors.

has been confirmed by MGCM simulation (Medvedev et al., 2015). Meanwhile, two density peaks appear at around 60 °S and 60 °N, where the zones are at the edges of the dust main peaks. Additionally, the south polar warming emerges at around 75 °S, hitting the yearly maximum with density of 3-5 times than other seasons. The polar warming is due to small-scale gravity waves heating and the coupling with the dust storms (Medvedev & Yiğit, 2012; Jain et al., 2020).

The winter has a warming equatorial region commonly located between 30 °S and 30 °N, sometimes even enlarging to 50 °S and 50 °N, hitting a relative maximum globally. Here we use the term 'Winter Equatorial Warming' to represent the warming. At the same time, the south polar warming is also located at the similar location to the autumn season, where the global density hit their annual maximum. Moreover, the WEW has latitudinal variations as shown in Figure 1 and Figure 2 (winter), where the density is relative lower than the one around 30 °S and 30 °N. The speciality of the WEM is that the winter dust peaks also happened around the equatorial area, however, the expansion of the CO2 and N2 are not cooling down the region in upper atmosphere.

The WEW could be owing to two factors by overview Figure 2. First, the trans-hemisphere circulation patterns have distinct seasonal evolution, which triggers the complex latitudinal variations from spring to winter (Figure 2, upper to lower panels). The overall structure of the WEW can be regarded as the result of the winter trans-hemispheric circulations in term of large-scale atmospheric dynamical processes. On the other hands, there are still latitudinal variations inside the WEW structure(Figure 1; lower panels of Figure 2b and 2c). The maximum inside the WEW could generated by the upwards small-scale gravity waves and the deep gills could be CO2 15 μm cooling by the atmospheric expansion due to winter local dust storms.

3.2 WEW in term of main species

Five main volatiles (CO2,Ar,CO,O,and N2) from NGIMS observations (Ls 270°-360°,Figure 3) are used to describe the WEW during MY32 to MY34, in which the MY34 was encountered with a global dust storm event during the autumn (Montabone et al., 2020; Jain et al., 2020). The seasonal trend of the species CO2,Ar,CO,and N2 are dominated by the function as illustrated in equation (1), which are similar with the seasonal evolution of the mass density (J. Liu et al., 2019). Meanwhile, the CO2 derivative, atomic

oxygen (O) are mostly forced by the solar term that is proportional to $\alpha_1 cosSZA + \alpha_2$ (Li et al., 2020), where the dust term seems have no influence on the seasonal variation of the volatile (Figure 3) (Gkouvelis et al., 2020; Li et al., 2020). Therefore, the global distribution of O is a good indicator to observe the solar heating and the corresponding trans-hemisphere circulation in upper layers.

The main WEW features are captured by CO2, Ar, CO, and N2 up to an altitude of at least 240 km (Figure 3b). For the first three volatiles, the latitude variation of the WEW is similar to each other (Figure 3), where two peaks located at around 30°N and 30°S. Additionally, the density around the equator is relatively lower than these two peaks (Figure 1a). The latitudinal structure of the WEW in N2 is not clear as the other three species, which the WEW maximum has southward shifting compared with other three species. The structure can be seen as trans-hemisphere circulation. Other characters include a south polar warming mainly heated by upward propagating small-scale gravity waves (Medvedev & Yiğit, 2012) as well as amplitude increasing enriched by winter dust storms (Elrod et al., 2020; Jain et al., 2020). An extremely warming north high-latitude region revealed by N2 as well as can be predicted by MGCM (Figure 1b). Two global minimum around 60°S and 60°N could be cooled by thermal effect, i.e., radiative transfer by CO2 in Infra-red band (Medvedev et al., 2015), specifically, CO2 backgrounding enhancement by the atmospheric expansion caused by autumn-winter dust storms (Montabone et al., 2020; Jain et al., 2020). Overall, heating by vertical gravity waves from lower layers and thermal cooling by fall-winter CO2 expansion are two key processes driving those warming-cooling structure.

The atomic oxygen (O) has a seasonal cycle that mainly forced by the solar term as described in Figure 4 and Li et al. (2020). The enrichment of the oxygen abundance during the fall-winter dust seasons is not observed from MY32 to MY34. This reflects that the volatile is a derivatives of CO2, which dissociated or ionized by the solar EUV flux and consumed by photochemical reactions within a few Martian months. The south polar warming and the cooling of around 60°S and 60°N region are also captured. Therefore, the atomic oxygen is sensitive to the two lower dynamical processes: CO2 expansion cooling and upward gravity waves heating. Other driver for the latitudinal variation of O can be owing to solar forcing (Elrod et al., 2020).

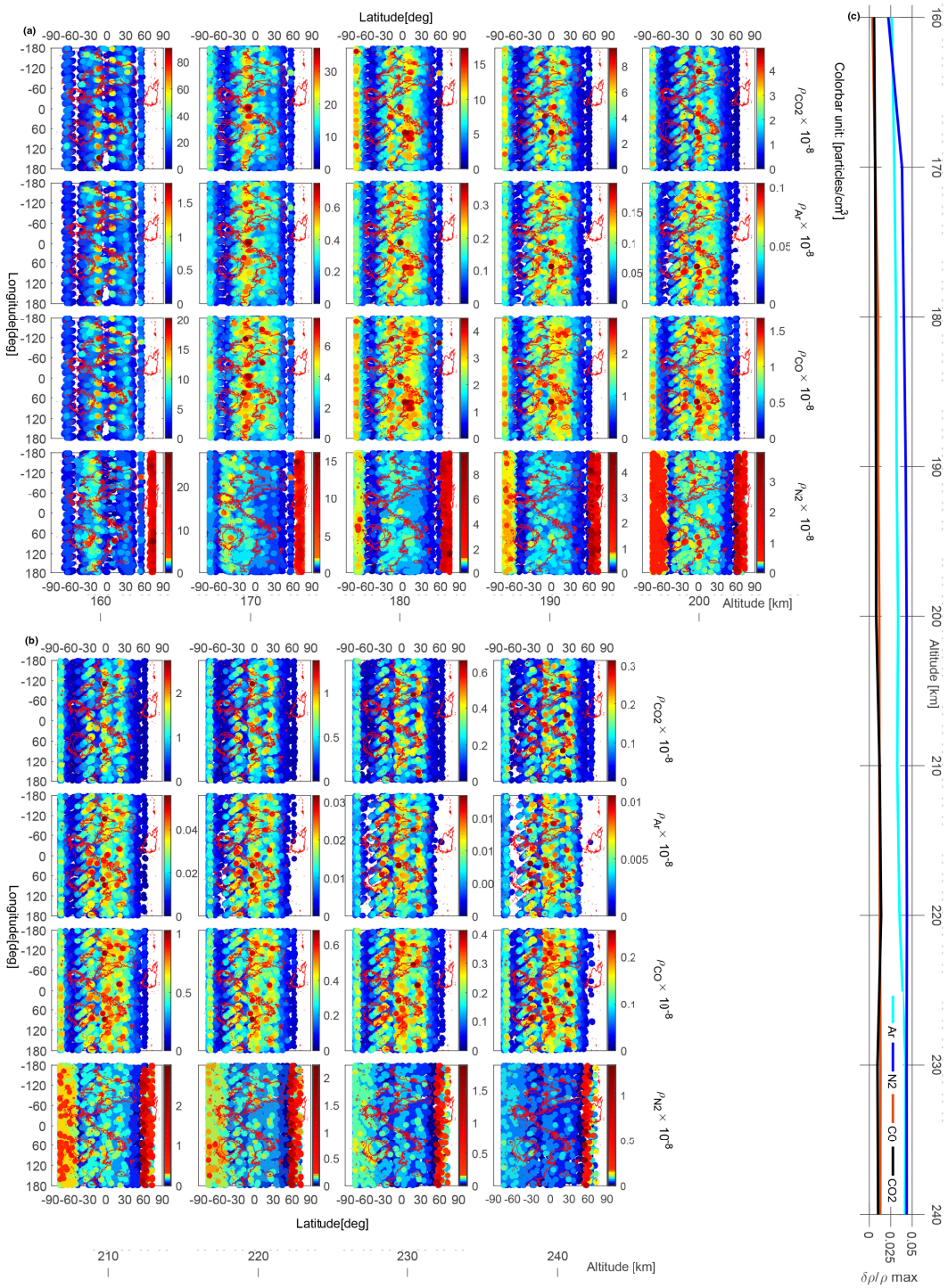

Figure 3. Winter global variation of NGIMS-measured species abundances. Panels upper to lower: [CO2,Ar,CO and N2]. (a) altitude from 160 to 200 km; (b) 210 to 240 km. (c) relative error maximum $\delta\rho/\rho$. Winter Equatorial Warming appeared at all the four volatiles from altitude 160 to 240 km. An extremely warming north polar area is reflected by N2. Note that the polar warming by N2 is several magnitude higher than the WEW, therefore, the colorbar is shifted to illustrate the equatorial sector. The latitude variation of the WEW is similar for CO2,Ar,and CO, where there are peaks around both 30°S and 30°N as well as a trough around the equator.

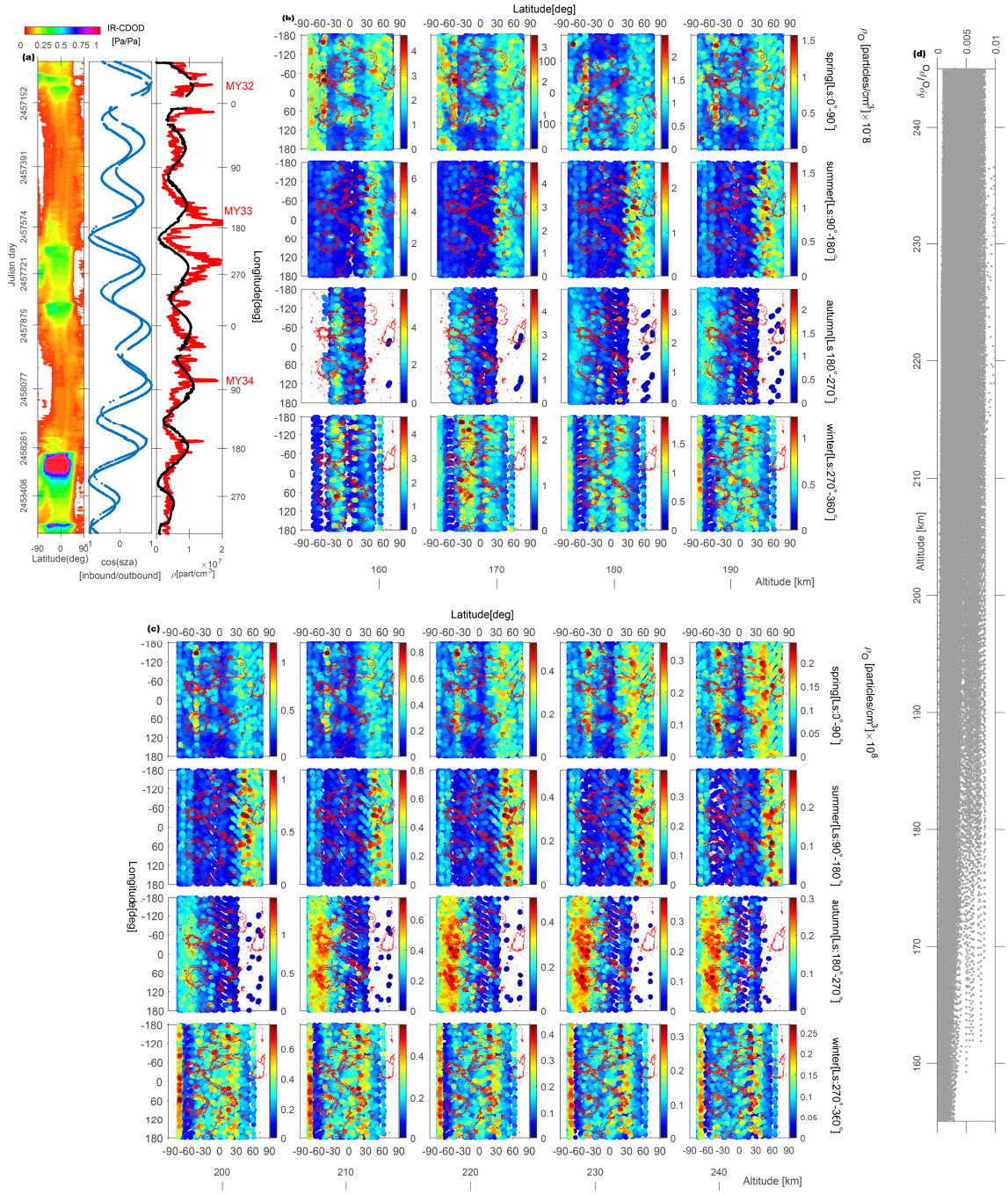

Figure 4. Atomic oxygen [O] distribution from 160-240 km of the four seasons. (a) The seasonal O abundance are tight related with the $cos(SZA)$ (shallow blue line) and fit by the solar term (black line). Not that two abnormal peaks exist between Ls 120° to 270 ° at MY33. No distinct correlation found between the IR-CDOD and measurements. (b) and (c): Global variation from 160 to 240 km. WEW and polar warming are also found during winter. (d) relative error $\delta\rho/\rho$.

The WEW feature reflected by the O experiences a fast vanishing in 20°S to 20°N during the night side (Figure 1a), which the abundance are extremely low (Figure 1a). At the same time, the night warming exists at around 30°S and 30°N with a width of 5 degree in latitude. The lower density is caused by the vanishing of solar UV heating during the night time and the CO2 radiative cooling (Stone et al., 2018, Figure 22). The warming feature could be due to solar near-IR heating and waves propagated from the dayside.

3.3 Orographic-related longitudinal structure

A wave-2 longitudinal structure has been found in the WEW region (30°S to 30°N), which is tightly correlated with the two-peaks Mars equatorial topography (Figure 5h). The structure is quite flat since the altitude is at around 170 km in the thermosphere. Formal researches describe the these longitudinal variations in term of tidal-wave theory (e.g., Moudden & Forbes, 2008; Lo et al., 2015; S. L. England et al., 2019, and others), regarding typical spring/summer longitudinal waves as a modulation of diurnal solar cycle with the two-trough Mars topography (wave-3) (Lo et al., 2015; Wu et al., 2015; S. L. England et al., 2019). Additionally, the autumn structure was seen as wave-4 planetary waves (Tolson et al., 2008; Moudden & Forbes, 2008; Wu et al., 2015) as well as the winter structure was regarded as wave-2 tidal waves by NGIMS N2 abundance (G. Liu et al., 2017) and IUVS observations (Schneider et al., 2020).

However, the winter equatorial longitudinal structure reflected by Figure 5 could be directly mountain effects. A strong evidence to gain insight into the dynamical nature of Mars atmosphere has been given by Benna et al. (2019) using the along-track winds, indicating that Mars whole atmosphere is highly influenced by the dissipation of the upward gravity waves (Yiğit et al., 2015). Currently, the LMD-MGCM can give wave-3 or wave-4 planetary wave prediction (Figure 5g) in the winter equatorial region but failed to simulate the mountain effect directly.

Complex perturbations are modulated with the orographic effects. The first source to trigger the variation is the upward propagation gravity waves (Moudden & Forbes, 2008; Benna et al., 2019), at the same time, heating up the upper layers. The second source is the solar-driven variations, which is reflected by the O (Figure 5e). The dust storms, together with the stronger zonal winds during the fall-winter season (Kuroda et al., 2020),

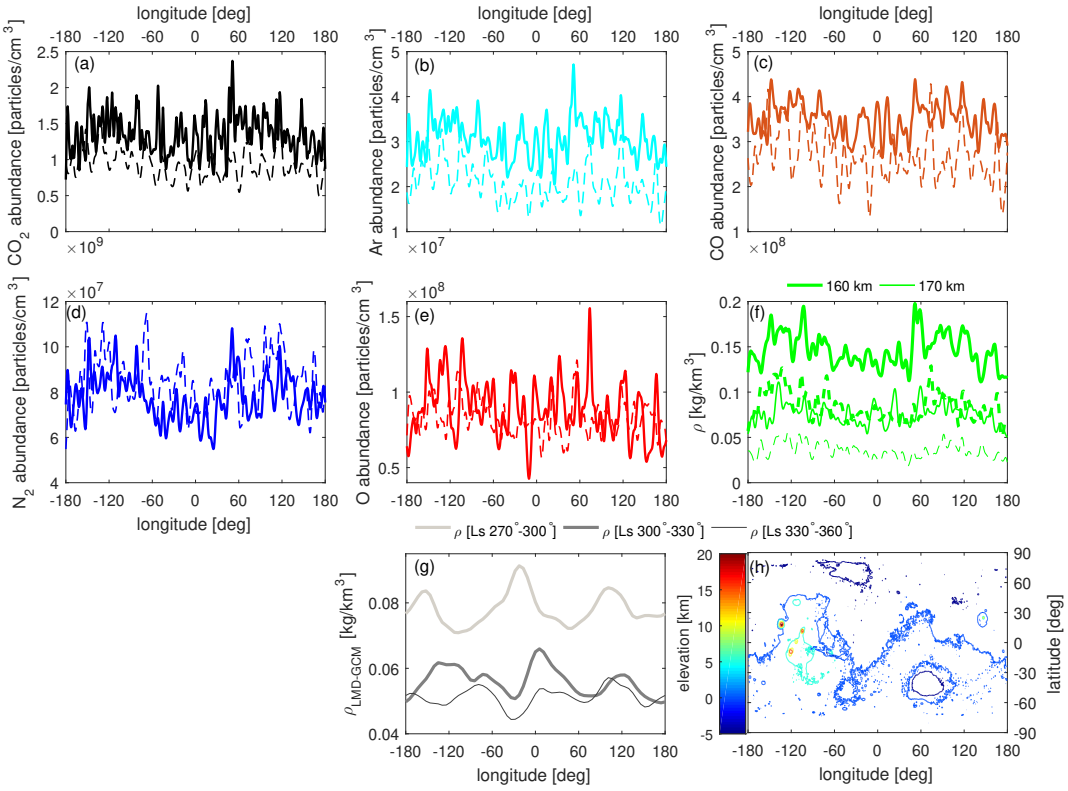

Figure 5. Longitudinal density (average) structure during NH winter (Ls: 270°-360°) at equatorial region (30°S to 30°N) at an altitude of 160 km. Solid lines: dayside; dash lines: nightside. The structure exists in (a) CO2,(b) Ar,(c) CO, (d) N2, and (f) mass density (green) except (e) atomic oxygen (O, red). The structure is tightly correlated with (h) Mars unique topography. Complex perturbations are modulated with the structure. (g) LMD-MGCM simulation has been made during Mars month 10, 11 ,and 12 and wave-3 and wave-4 structure have been found. The topographic-effect cannot be recovered by the current model.

could be important contributor to the mountain effects. These non-orographic generated gravity waves could contribute warming effect in 20°S to 20°N around solstice periods (Gilli et al., 2020).

4 What Are the Triggers of WEW?

4.1 Trans-hemispheric circulations of upper layers

The seasonal evolution of Mars upper layers as shown in Figure 6 and equation (1) results in changing of the trans-hemispheric circulation, which could be the large-scale and long-term factor that regulates the appearances of winter equatorial warming and latitudinal variations of other three seasons of Mars upper atmosphere. The warming spring north hemisphere and the banded summer longitudinal structure (Figure 2 and 4, summer) are good indicator to illustrate the seasonal circulation patterns' evolution. The main peaks of seasonal dust storms during autumn (Montabone et al., 2020) caused atmospheric inflations (Gkouvelis et al., 2020) up to beyond the exobase (Elrod et al., 2020; Fang et al., 2020), in which the background CO2 generated a extremely cold autumn equator(Figure 2 and Figure 4, autumn) (Medvedev et al., 2015; Gilli et al., 2020). S. Bougher et al. (2006, and others) were also owing polar warming to this mechanism.

4.2 Local factors

Small-scale upward gravity waves heating originated from orographic (Benna et al., 2019) or non-orographic sources (Gilli et al., 2020) as well as the CO2 15 μm cooling (Medvedev et al., 2015) were thought to be the another two major triggers that could influence the upper layers from lower atmosphere. The polar warming are thought to be major caused by upward gravity waves heating and corresponding dust impacts coupling in high-latitude region (Medvedev & Yiğit, 2012). We have observed the phenomenon in Figure 1, 2,3,4 and 5. The cooling in 40°-60° region are mainly caused by CO2 IR radiative transfer, which have been valid by MGCM simulations (Medvedev & Yiğit, 2012; Medvedev et al., 2015). The same reason could explain the density dropping inside the WEW structure (Figure 1,2,3,4). High-resolution MGCM simulations shown that the global dust storms like MY34 can expand the gravity waves amplitudes 2 times more than the quiet seasons by changing the trans-hemisphere circulation in term of zonal wind perturba-

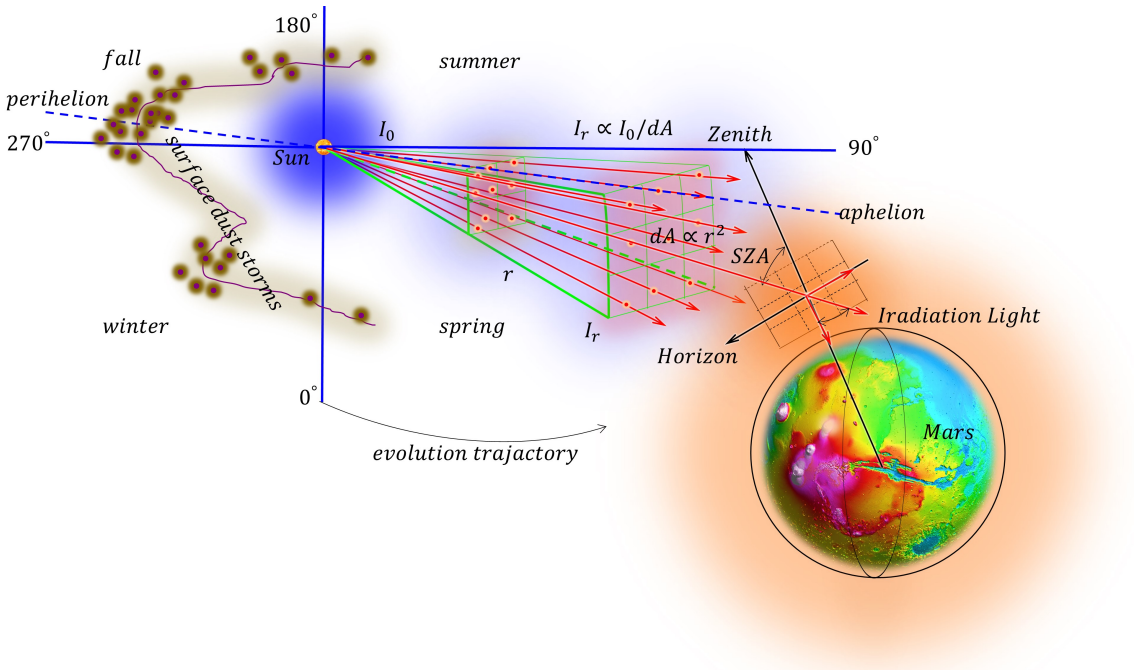

Figure 6. Seasonal evolution of Mars upper atmosphere governed by the astronomical tides and the local surface dust storms. The Mars upper atmosphere (shallow yellow glow) is driven by both solar irradiation (blue glow) and surface events such as dust storms (purple line with glow and dusty dots where the numbers of the dots symbolize the activeness of the storms.). The fluxes (red arrow) originated from solar (the intensity is represented by I_0) propagate through the planetary space with a decreasing strength that is proportional to ($\propto$) the inverse square of the distance (r), i.e., $I_r \propto I_0/r^2$. Around the Mars nearby space, the atmospheric volatiles are major forced by the zenith component that is pointing to the Martian geo-center and is proportional to $I_r cos SZA$, where SZA is the first letter of the abbreviation of Solar Zenith Angle. At the same time, the upper layers are also impacted by the surface dust activities started at end of the north hemisphere summer ($Ls \approx 135^o$) during the seasonal evolution, in which the atmospheric density could increase a factor of 2 to 3 times (Gkouvelis et al., 2020) higher than that of quiet seasons ($Ls \approx 0^o - 135^o$). This mechanism is expressed by equation (1).

tions (Kuroda et al., 2020). The density perturbations growing during autumn-winter dust seasons can also be captured by MAVEN densities (Li et al., 2020).

By comparing the day and night O WEW structure (Figure 1 and 5), we notice that the density trough inside the structure experienced longitudinal expanding toward the polar during the nightside, which shows that the solar heating do have strong influence on the O WEW. The longitudinal variation of the WEW shows that large-scale dynamical process such as topographic effect could be another important factor that could influence the winter equatorial density distribution.

4.3 Limitations of the current simulations

We have done several LMD-MGCM simulations in various scenarios (i.e., different solar conditions and dust storms). The above trans-hemisphere circulation and local factors regulated features are all can be repeated in spring to autumn with high accuracy. The winter polar warming are also reproduced, which is correlated with the observations shown in Figure 1 and other figures. The sub-grid effects are not well-integrated with the LMD-MGCM, though the primitively simulation of non-orographic generated gravity waves do have heating effect to the winter equatorial region (Gilli et al., 2020). The winter wave-2 structure are not available by the simulation (Figure 5g). The lower dynamical processes such as topographic effects on the upper layers might need to be further considered.

5 Summary

The Mars Winter Equatorial Warming (WEW) is reported by accelerometer-derived and NGIMS-measured densities (CO2,Ar,CO,N2,and O). The overall picture of the WEW is defined by the mass density firstly. The phenomenon is also detected, together with the polar warming, by the main species. The drivers of the seasonal evolution of the upper atmospheric density are analysed, in which we found that: (1) the WEW can be regarded as a winter trans-hemispheric circulation pattern. The circulation is driven by yearly solar-insolation evolution and the impacts of the seasonal surface dust storms. (2) The latitudinal variation inside the WEW structure, could be caused by the inflation of lower atmospheric layers' CO2 and N2 during the dust seasons (cooling effects, density decrease) as well as the heating effects could be caused by the upward small-scale grav-

ity waves. (3) The longitudinal variation of the WEW is a wave-2 structure, which is clearly detected by both mass density and other four species (CO2,Ar,CO,N2) below 170 km. The structure is tightly orographic-related, which could suggest that the Mars atmosphere is much more 'dynamical' than we expected. The topographic-related wave-2 variation, to some extent, is coincided with the along tracks winds retrieves as shown by Benna et al. (2019) and the simulation made by (Kuroda et al., 2020).

Acknowledgments

The paper is supported by The Startup Foundation for Introducing Talent of NUIST (Grant No: 2019r089) and Key Laboratory of Planetary Sciences Project (Grant No: PSL_1607). This work made use of the High Performance Computing Resource in the Core Facility for Advanced Research Computing at Shanghai Astronomical Observatory. The density data are provided by NASA Planetary Data System (PDS) (`https://pds-atmospheres.nmsu.edu/data_and_services/atmospheres_data/MARS/mars_orbiter.html`). The simulation made by this paper using the Mars General Circulation Model and Mars Climate Database developed in Laboratoire de Météorologie Dynamique.

References

Benna, M., Bougher, S., Lee, Y., Roeten, K., Yiğit, E., Mahaffy, P., & Jakosky, B. (2019). Global circulation of mars' upper atmosphere. *Science*, *366*(6471), 1363–1366.

Bougher, S., Bell, J., Murphy, J., Lopez-Valverde, M., & Withers, P. (2006). Polar warming in the mars thermosphere: Seasonal variations owing to changing insolation and dust distributions. *Geophysical Research Letters*, *33*(2).

Bougher, S. W., Roeten, K. J., Olsen, K., Mahaffy, P. R., Benna, M., Elrod, M., ... others (2017). The structure and variability of mars dayside thermosphere from maven ngims and iuvs measurements: Seasonal and solar activity trends in scale heights and temperatures. *Journal of Geophysical Research: Space Physics*, *122*(1), 1296–1313.

Elrod, M., Bougher, S., Roeten, K., Sharrar, R., & Murphy, J. (2020). Structural and compositional changes in the upper atmosphere related to the pede-2018 dust event on mars as observed by maven ngims. *Geophysical Research Letters*, *47*(4), e2019GL084378.

354 England, S., Liu, G., Yiğit, E., Mahaffy, P., Elrod, M., Benna, M., ... Jakosky, B.
355 (2017). Maven ngims observations of atmospheric gravity waves in the mar-
356 tian thermosphere. *Journal of Geophysical Research: Space Physics*, *122*(2),
357 2310–2335.

358 England, S. L., Liu, G., Kumar, A., Mahaffy, P. R., Elrod, M., Benna, M., ... oth-
359 ers (2019). Atmospheric tides at high latitudes in the martian upper atmo-
360 sphere observed by maven and mro. *Journal of Geophysical Research: Space*
361 *Physics*, *124*(4), 2943–2953.

362 Fang, X., Ma, Y., Lee, Y., Bougher, S., Liu, G., Benna, M., ... others (2020). Mars
363 dust storm effects in the ionosphere and magnetosphere and implications for
364 atmospheric carbon loss. *J. Geophys. Res. Space Phys*, *125*.

365 Felici, M., Withers, P., Smith, M., González-Galindo, F., Oudrhiri, K., & Kahan,
366 D. (2020). Maven rose observations of the response of the martian ionosphere
367 to dust storms. *Journal of Geophysical Research: Space Physics*, *125*(6),
368 e2019JA027083.

369 Forbes, J. M., Bridger, A. F., Bougher, S. W., Hagan, M. E., Hollingsworth, J. L.,
370 Keating, G. M., & Murphy, J. (2002). Nonmigrating tides in the thermosphere
371 of mars. *Journal of Geophysical Research: Planets*, *107*(E11), 23–1.

372 Forbes, J. M., & Zhang, X. (2018). Polar region variability in the lower thermo-
373 sphere of mars from odyssey and reconnaissance orbiter aerobraking measure-
374 ments. *Journal of Geophysical Research: Space Physics*, *123*(10), 8664–8687.

375 Gilli, G., Forget, F., Spiga, A., Navarro, T., Millour, E., Montabone, L., ...
376 Schofield, J. (2020). Impact of gravity waves on the middle atmosphere of
377 mars: A non-orographic gravity wave parameterization based on global climate
378 modeling and mcs observations. *Journal of Geophysical Research: Planets*,
379 *125*(3), e2018JE005873.

380 Gkouvelis, L., Gérard, J.-C., González-Galindo, F., Hubert, B., & Schneider, N.
381 (2020). Isobar altitude variations in the upper mesosphere observed with
382 iuvs-maven in response to martian dust storms. *Geophysical Research Letters*,
383 *47*(12), e2020GL087468.

384 Jain, S., Bougher, S., Deighan, J., Schneider, N., González Galindo, F., Stewart, A.,
385 ... Pawlowski, D. (2020). Martian thermospheric warming associated with
386 the planet encircling dust event of 2018. *Geophysical Research Letters*, *47*(3),

e2019GL085302.

Jakosky, B. M., Grebowsky, J. M., Luhmann, J. G., Connerney, J., Eparvier, F., Ergun, R., ... others (2015). Maven observations of the response of mars to an interplanetary coronal mass ejection. *Science*, *350*(6261).

Jakosky, B. M., Lin, R., Grebowsky, J., Luhmann, J., Mitchell, D., Beutelschies, G., ... others (2015). The mars atmosphere and volatile evolution (maven) mission. *Space Science Reviews*, *195*(1-4), 3–48.

Keating, G., Bougher, S., Zurek, R., Tolson, R., Cancro, G., Noll, S., ... others (1998). The structure of the upper atmosphere of mars: In situ accelerometer measurements from mars global surveyor. *Science*, *279*(5357), 1672–1676.

Keating, G., Theriot, M., Tolson, R., Bougher, S., Forget, F., & Forbes, J. (2003). Brief review on the results obtained with the mgs and mars odyssey 2001 accelerometer experiments. In *Proceedings, international workshop: Mars atmosphere modeling and observations, granada, spain* (pp. 13–15).

Kuroda, T., Medvedev, A. S., & Yiğit, E. (2020). Gravity wave activity in the atmosphere of mars during the 2018 global dust storm: Simulations with a high-resolution model. *Journal of Geophysical Research: Planets*, e2020JE006556.

Li, Y., Liu, J., & Jin, S. (2020). Horizontal internal gravity waves in the mars upper atmosphere from maven acc and ngims measurements. *Journal of Geophysical Research: Space Physics*, *126*(1), e2020JA028378.

Liu, G., England, S., Lillis, R. J., Mahaffy, P. R., Elrod, M., Benna, M., & Jakosky, B. (2017). Longitudinal structures in mars' upper atmosphere as observed by maven/ngims. *Journal of Geophysical Research: Space Physics*, *122*(1), 1258–1268.

Liu, J., Jin, S., & Li, Y. (2019). Seasonal variations and global wave distributions in the mars thermosphere from maven and multisatellites accelerometer-derived mass densities. *Journal of Geophysical Research: Space Physics*, *124*(11), 9315–9334.

Lo, D. Y., Yelle, R. V., Schneider, N. M., Jain, S. K., Stewart, A. I. F., England, S. L., ... others (2015). Nonmigrating tides in the martian atmosphere as observed by maven iuvs. *Geophysical Research Letters*, *42*(21), 9057–9063.

Mahaffy, P. R., Benna, M., Elrod, M., Yelle, R. V., Bougher, S. W., Stone, S. W., & Jakosky, B. M. (2015). Structure and composition of the neutral upper

atmosphere of mars from the maven ngims investigation. *Geophysical research letters*, *42*(21), 8951–8957.

Medvedev, A. S., González-Galindo, F., Yiğit, E., Feofilov, A. G., Forget, F., & Hartogh, P. (2015). Cooling of the martian thermosphere by co2 radiation and gravity waves: An intercomparison study with two general circulation models. *Journal of Geophysical Research: Planets*, *120*(5), 913–927.

Medvedev, A. S., Nakagawa, H., Mockel, C., Yiğit, E., Kuroda, T., Hartogh, P., ... others (2016). Comparison of the martian thermospheric density and temperature from iuvs/maven data and general circulation modeling. *Geophysical Research Letters*, *43*(7), 3095–3104.

Medvedev, A. S., & Yiğit, E. (2012). Thermal effects of internal gravity waves in the martian upper atmosphere. *Geophysical Research Letters*, *39*(5).

Montabone, L., Forget, F., Millour, E., Wilson, R., Lewis, S., Cantor, B., ... others (2015). Eight-year climatology of dust optical depth on mars. *Icarus*, *251*, 65–95.

Montabone, L., Spiga, A., Kass, D. M., Kleinböhl, A., Forget, F., & Millour, E. (2020). Martian year 34 column dust climatology from mars climate sounder observations: Reconstructed maps and model simulations. *Journal of Geophysical Research: Planets*, e2019JE006111.

Moudden, Y., & Forbes, J. (2008). Topographic connections with density waves in mars' aerobraking regime. *Journal of Geophysical Research: Planets*, *113*(E11).

Schneider, N. M., Milby, Z., Jain, S., González-Galindo, F., Royer, E., Gérard, J.-C., ... others (2020). Imaging of martian circulation patterns and atmospheric tides through maven/iuvs nightglow observations. *Journal of Geophysical Research: Space Physics*, *125*(8), e2019JA027318.

Stone, S. W., Yelle, R. V., Benna, M., Elrod, M. K., & Mahaffy, P. R. (2018). Thermal structure of the martian upper atmosphere from maven ngims. *Journal of Geophysical Research: Planets*, *123*(11), 2842–2867.

Terada, N., Leblanc, F., Nakagawa, H., Medvedev, A. S., Yiğit, E., Kuroda, T., ... others (2017). Global distribution and parameter dependences of gravity wave activity in the martian upper thermosphere derived from maven/ngims observations. *Journal of Geophysical Research: Space Physics*, *122*(2), 2374–2397.

Thaller, S. A., Andersson, L., Pilinski, M. D., Thiemann, E., Withers, P., Elrod, M., ... Jenkins, G. (2020). Tidal wave-driven variability in the mars ionosphere-thermosphere system. *Atmosphere*, *11*(5), 521.

Tolson, R., Bemis, E., Hough, S., Zaleski, K., Keating, G., Shidner, J., ... Thomas, P. (2008). Atmospheric modeling using accelerometer data during mars reconnaissance orbiter aerobraking operations. *Journal of Spacecraft and Rockets*, *45*(3), 511–518.

Withers, P. (2006). Mars global surveyor and mars odyssey accelerometer observations of the martian upper atmosphere during aerobraking. *Geophysical research letters*, *33*(2).

Wu, Z., Li, T., & Dou, X. (2015). Seasonal variation of martian middle atmosphere tides observed by the mars climate sounder. *Journal of Geophysical Research: Planets*, *120*(12), 2206–2223.

Yiğit, E., England, S. L., Liu, G., Medvedev, A. S., Mahaffy, P. R., Kuroda, T., & Jakosky, B. M. (2015). High-altitude gravity waves in the martian thermosphere observed by maven/ngims and modeled by a gravity wave scheme. *Geophysical Research Letters*, *42*(21), 8993–9000.

Zurek, R., Tolson, R., Bougher, S., Lugo, R., Baird, D., Bell, J., & Jakosky, B. (2017). Mars thermosphere as seen in maven accelerometer data. *Journal of Geophysical Research: Space Physics*, *122*(3), 3798–3814.

Zurek, R. W., Tolson, R. H., Baird, D., Johnson, M. Z., & Bougher, S. W. (2015). Application of maven accelerometer and attitude control data to mars atmospheric characterization. *Space Science Reviews*, *195*(1-4), 303–317.